

¹ Local host tree density increases forest insect disturbance severity,
² but host size effect depends on climatic water deficit

³ Michael J. Koontz^{1,2,*}, Andrew M. Latimer^{1,2}, Leif A. Mortenson³, Christopher J. Fettig³, Malcolm P.
⁴ North^{1,2,4}

⁵ ¹Graduate Group in Ecology, University of California, Davis, CA, USA

⁶ ²Department of Plant Sciences, University of California, Davis, CA, USA

⁷ ³USDA Forest Service, Pacific Southwest Research Station, Placerville, CA, USA

⁸ ⁴USDA Forest Service, Pacific Southwest Research Station, Davis, CA, USA

⁹ *Correspondence: michael.koontz@colorado.edu

¹⁰ Date report generated: April 10, 2019

¹¹ Executive Summary (to eventually become abstract)

¹² Framing: environmental drivers of insect severity, forest structure drivers of insect severity, but *complex* forest
¹³ structure is key as is relevant scale of local ecological process; little information on how the complex forest
¹⁴ structure interacts with environmental drivers because these data are challenging to capture simultaneously...

¹⁵ Bark beetles are a primary mortality agent of trees in western U.S. forests, and the recent Californian hot
¹⁶ drought of 2012 to 2015 created favorable conditions for bark beetle-induced tree mortality throughout the
¹⁷ yellow pine/mixed-conifer forest system in the Sierra Nevada mountain range. The western pine beetle,
¹⁸ *Dendroctonus brevicomis*, is the forest insect that is largely responsible for the especially common deaths of its
¹⁹ main host in California, the ponderosa pine tree (*Pinus ponderosa*). While previous work has demonstrated a
²⁰ link between climate conditions related to tree water stress and forest density on the severity of the western
²¹ pine beetle disturbance, it remains challenging to disentangle the relative effects of these variables. Further,
²² forest density can affect western pine beetle behavior in a number of ways, which creates a need for more
²³ information on complex forest structure (including local density, tree size, and the heterogeneity of these
²⁴ variables across a forest stand) to uncover the most likely mechanism.

²⁵ We conducted aerial surveys over an established network of 32 permanent vegetation monitoring plots along
²⁶ a 350km and 1000m elevation gradient in the Sierra Nevada mountain range of California using a small,
²⁷ unhumanned aerial system (sUAS aka drone) equipped with a narrow-band multispectral camera. Using
²⁸ Structure from Motion (SfM) processing on over 450,000 images, we reconstructed the complex vegetation
²⁹ structure of over 9 square kilometers of forest that experienced ponderosa pine mortality as a result of

western pine beetle activity. Using this dataset, we built a model to predict the probability of ponderosa pine mortality as a function of forest structure variables (including ponderosa pine density and mean size, as well as all tree density and mean size), an environmental gradient of climatic water deficit, and a Gaussian process to capture spatial covariance in the response.

Data from small, unhumanned aerial systems (sUAS) can provide important context surrounding ground plots, which enables inference and generates new insights into ecological processes. sUAS are best-suited to enhancing ground data, which implies that we need not abandon lessons learned from sound experimental design (i.e., a network of plots along a gradient is still a powerful way to use sUAS as an ecological tool).

Host availability for aggressive bark beetles appears to have played the dominant role in increasing the probability of ponderosa pine mortality in the most hard-hit forest stands during the cumulative mortality event of 2012 to 2018. Host size played a role in its interaction with environmental condition— climatic water deficit— such that numerous and smaller host trees increased the probability of ponderosa mortality at cool/wet sites, while numerous and larger host trees increased the probability of ponderosa mortality at hot/dry sites.

Our results corroborate the role of host tree density and regional climate conditions on the severity of forest insect disturbance, but also highlight the importance of complex forest structure (i.e., both host density and average host size) in its interaction with regional climate. Thus, the future forest structure may be affected differently by a large-scale forest insect disturbance for the same host tree/forest insect pairing, and during the same extreme drought, but across a gradient of regional climate conditions.

Introduction

Aggressive bark beetles dealt the final blow to many of the nearly 150 million trees killed in the California drought of 2012 to 2015 and its aftermath (USDAFS 2019). A harbinger of climate change effects to come, record high temperatures exacerbating the drought (Griffin and Anchukaitis 2014) increased water stress on trees, which increases their susceptibility to attacking bark beetles (Fettig 2012, Kolb et al. 2016). A century of fire suppression policy has enabled forests to grow into dense stands, which also makes them more vulnerable to bark beetle attack (Fettig 2012, North et al. 2015). This combination of environmental conditions and forest structural characteristics led to tree mortality events of unprecedented size in the driest, densest forests across the state (Young et al. 2017). The mechanisms underlying the link between tree susceptibility to insect attack and hot, dry conditions are often directly attributed to tree physiology (Bentz et al. 2010), but the link to forest density is multifaceted (Fettig 2012). Because forest density is a coarse metric

60 of the complex forest structure to which bark beetles respond (Raffa et al. 2008), our understanding of the
61 connection between forest density and insect disturbance severity may be enhanced with more finely-resolved
62 measures of forest structure (Stephenson et al. 2019). Further, the interaction between local-scale complex
63 forest structure and broad-scale environmental conditions as they affect forest insect disturbance remains
64 underexplored (Seidl et al. 2016).

65 The yellow pine/mixed-conifer forests in California's Sierra Nevada region are characterized by regular bark
66 beetle disturbances, primarily by the western pine beetle (*Dendroctonus brevicomis*) and its main host in the
67 system, ponderosa pine (*Pinus ponderosa*) (Fettig et al. 2019). The western pine beetle is a "primary" or
68 "aggressive" bark beetle, with reproductive success contingent upon host tree mortality (Raffa and Berryman
69 1983, Fettig et al. 2019). This strong Allee effect creates a dynamic between beetle host selection behavior
70 and host tree susceptibility to attack (Raffa and Berryman 1983, Logan et al. 1998). Under normal conditions,
71 primary bark beetles like the western pine beetle will sporadically kill weakened trees, but under outbreak
72 conditions, wide swaths of even healthy trees may be killed (Bentz et al. 2010, Raffa et al. 2015). A key
73 defense mechanism of trees to bark beetle attack is to flood beetle bore holes with resin, which physically
74 expels beetles and may interrupt beetle communication (Raffa et al. 2015). Under severe water stress, trees
75 may no longer have the resources available to mount this defense (Kolb et al. 2016) and thus prolonged
76 drought can often trigger increased bark beetle-induced tree mortality as average tree vigor declines (Bentz
77 et al. 2010).

78 Forest structure— the spatial distribution, size, and species composition of trees— also strongly influences
79 western pine beetle activity. For instance, high-density forests are more prone to bark beetle attacks, and
80 several mechanism likely underlie this phenomenon (Fettig 2012). A high-density forest may experience greater
81 bark beetle-induced tree mortality because host availability is high and shorter dispersal distances facilitate
82 successful colonization of those hosts (Miller and Keen 1960, Berryman 1982, Fettig et al. 2007), because
83 high host availability reduces the chance of landing on a non-host and imposing an energy cost to individual
84 beetles (Moeck et al. 1981, Evenden et al. 2014), because crowded trees experience greater competition
85 for water resources and thus average tree resistance is lower (Hayes et al. 2009), or because smaller gaps
86 between trees protect pheromone plumes from dissipation by the wind and thus enhance intraspecific beetle
87 communication (Thistle et al. 2004). Additionally, tree size affects bark beetle host selection behavior as
88 smaller trees tend to have less capacity for resisting attack, but larger trees represent a more desirable target
89 because their thicker phloem provides greater nutritional value (Chubaty et al. 2009, Graf et al. 2012). Tree
90 density thus paints a fundamentally limited picture of the mechanism by which forest structure affects bark
91 beetle disturbance, but *complex* forest structure— with explicit recognition of tree size, species composition

92 (e.g., host versus non-host composition), and variability in local tree density—should more appropriately
93 capture the ecological processes underlying insect-induced tree mortality. Additionally, considering the effects
94 of complex forest structure simultaneously to the effects of environmental conditions may help refine our
95 understanding of observed patterns of tree mortality in the recent California hot drought.

96 The vast spatial extent of tree mortality in the 2012 to 2015 California hot drought (USDAFS 2019) challenges
97 our ability to simultaneously consider how broad-scale environmental conditions may interact with local,
98 complex forest structure to affect the dynamic between bark beetle host selection and host tree susceptibility
99 to attack (Stephenson et al. 2019). Measuring complex forest structure generally requires expensive equipment
100 or labor-intensive field surveys (Larson and Churchill 2012, Kane et al. 2014, Asner et al. 2016), which
101 constrains survey extent and frequency. Small, unhumanned aerial systems (sUAS) enable relatively fast and
102 cheap remote imaging over dozens of hectares of forest, which can be used to determine both forest structure
103 and tree condition at the individual tree scale (Morris et al. 2017, Shiklomanov et al. 2019). Distributing such
104 surveys across an environmental gradient is a viable approach to overcoming the data acquisition challenge
105 inherent in investigating multi-scale phenomonena.

106 We used ultra-high resolution remote sensing data from a small, unhumanned aerial system over a network of
107 32 sites in the Sierra Nevada spanning 1000m of elevation and 350km of latitude and covering a total of 9
108 square kilometers of forest to ask how broad-scale environmental conditions interacted with local, complex
109 forest structure to affect the probability of tree mortality during the cumulative mortality event of 2012 to
110 2018. We asked:

- 111 1. How does local host tree density and size affect the severity of western pine beetle disturbance?
- 112 2. How does total tree density and size affect the severity of western pine beetle disturbance?
- 113 3. How does environmentally-driven tree moisture stress affect the severity of western pine beetle distur-
114 bance?
- 115 4. Do the effects of forest structure and environmental condition on western pine beetle disturbance
116 interact?

117 Methods

118 Study system

119 The study sites comprise mostly ponderosa pine trees, *Pinus ponderosa*, whose primary bark beetle predator
120 in California is the western pine beetle (WPB), *Dendroctonus brevicomis*. The WPB is an aggressive bark

121 beetle, meaning it must attack and kill live trees in order to successfully reproduce (Raffa et al. 2008).
122 Pioneer WPBs disperse to a new host tree, determine the host's susceptibility to attack, and use pheromone
123 signals to attract other WPBs. The attracted WPBs mass attack the tree by boring into its inner bark,
124 laying eggs, and dying, leaving their offspring to develop inside the doomed tree before themselves dispersing
125 (Raffa et al. 2008). Small WPB populations prefer weakened trees but large populations can overwhelm
126 the defense mechanisms of even healthy trees. Successful attacks on large, healthy trees are boons to bark
127 beetle fecundity and trigger outbreaks in which populations explode and massive tree mortality occurs. In
128 California, the WPB can have 3 generations in a single year giving it a greater potential to spread rapidly
129 through forests than its more infamous congener, the mountain pine beetle, *Dendroctonus ponderosa* (MPB).

130 We built our study on 180 vegetation/forest insect monitoring plots at 36 sites established between 2016 and
131 2017 (Fettig et al. 2019). These established plots were located in beetle-attacked, mixed-conifer forests across
132 the Eldorado, Stanislaus, Sierra and Sequoia National Forests and were stratified by elevation (914-1219
133 meters [3000-4000 feet], 1219-1524 meters [4000-5000 feet], 1524-1828 meters [5000-6000 feet] above sea level).
134 In the Sequoia National Forest, the National Forest that is furthest south, plots were stratified with the lowest
135 elevation band between 1219 and 1524 (4000-5000 feet) and extended to an upper elevation band of 1828-2133
136 (6000-7000 feet) to capture a more similar forest community composition as at the more northern National
137 Forests. The sites have variable forest structure and disturbance history and plot locations were selected
138 specifically in areas with >40% ponderosa pine basal area and >10% ponderosa pine mortality. The 0.04ha
139 circular plots are clustered along transects in groups of 5, with between 80 and 200m between each plot. All
140 trees within the plot were assessed as dead or alive. The stem location of all trees was mapped relative to the
141 center of each plot using azimuth/distance measurements. Tree identity to species and diameter at breast
142 height (dbh) were recorded if dbh was greater than 6.35cm. During the spring and early summer of 2018, all
143 field plots were revisited to assess whether dead trees had fallen (Fettig et al. 2019).

144 **Instrumentation**

145 Imagery was captured using a DJI Zenmuse X3 RGB camera (DJI 2015a) and a Micasense RedEdge3 5-band
146 multispectral camera (Micasense 2015). We mounted both of these instruments simultaneously on a DJI
147 Matrice 100 aircraft (DJI 2015b) using the DJI 3-axis stabilized gimbal for the Zenmuse X3 camera and a
148 Micasense angled fixed mount for the RedEdge3 camera. The gimbal and the angled fixed mount ensured
149 both instruments were nadir-facing during image capture. Just prior or after image capture at each site, we
150 calibrated the RedEdge3 camera by taking an image of a calibration panel on the ground in full sun with
151 known reflectance values for each of the 5 narrow bands.

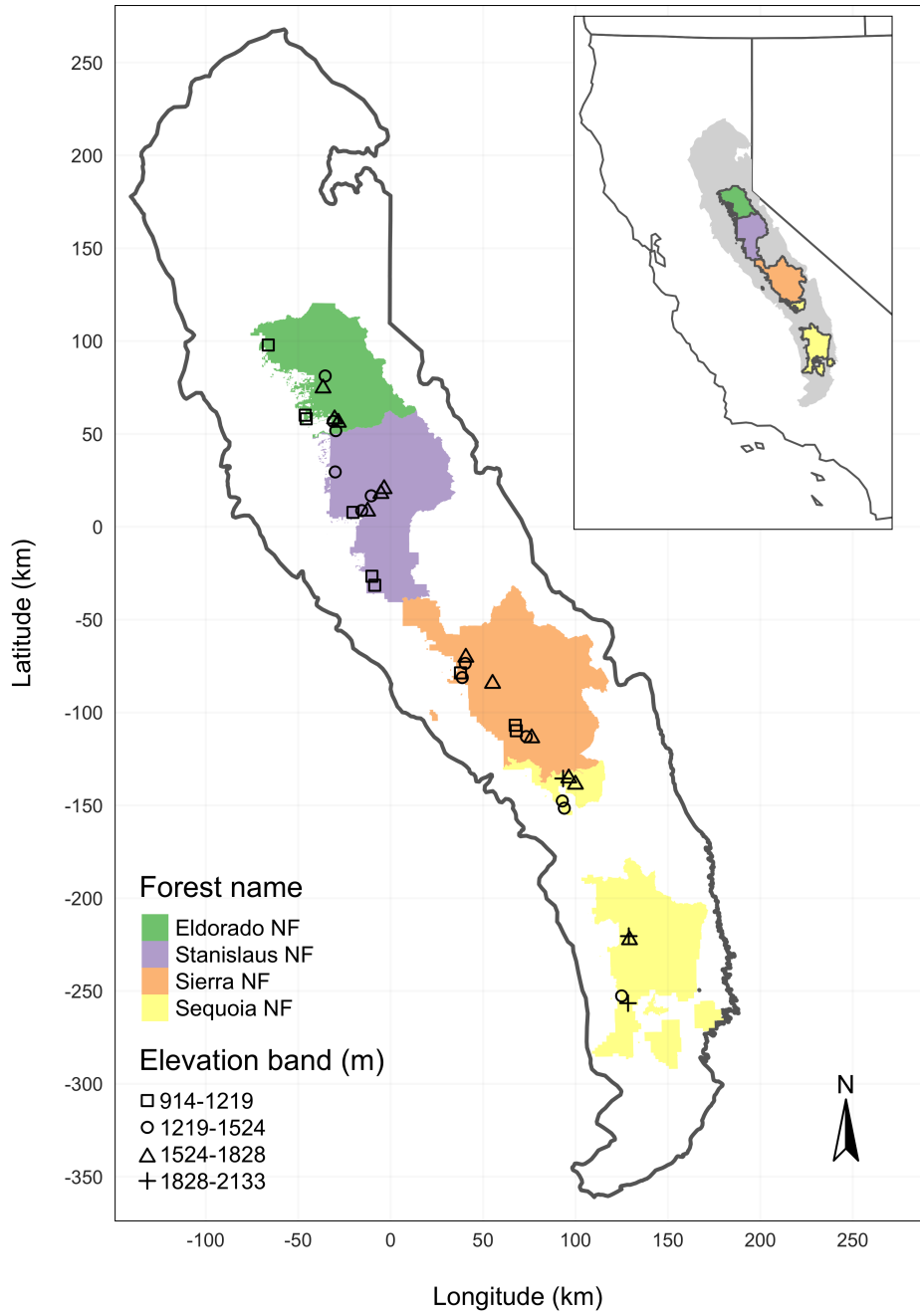


Figure 1: The network of field plots spanned a 350 km latitudinal gradient from the Eldorado National Forest in the north to the Sequoia National Forest in the south. Plots were stratified by three elevation bands in each forest, with the plots in the Sequoia National Forest (the southern-most National Forest) occupying elevation bands 305m above the three bands in the other National Forests in order to capture a similar community composition.

Table 1: Reflectance sensitivity of the Micasense Rededge3 camera. The calibration panel value represents the reflectance of the calibration panel for the given wavelength.

Band number	Band name	Center wavelength	Band width	Wavelength range	Panel reflectance
1	blue (b)	475	20	465-485	0.64
2	green (g)	560	20	550-570	0.64
3	red (r)	668	10	663-673	0.64
4	near infrared (nir)	840	40	820-860	0.6
5	red edge (re)	717	10	712-722	0.63

152 Flight protocol

153 Image capture was conducted as close to solar noon as possible to minimize shadow effects (always within 4
 154 hours; usually within 2 hours). Prior to the aerial survey, two strips of bright orange drop cloth (~100cm x
 155 15cm) were positioned as an “X” over the permanent monuments marking the center of the 5 field plots from
 156 Fettig et al. (2019).

157 For each of the 36 sites (containing 5 plots each), we captured imagery over the surrounding ~40 hectares of
 158 forested area using north-south aerial transects. For three sites, we surveyed less surrounding area in order to
 159 maintain visual and radio communication with the aircraft during flight which can be obstructed by steep
 160 terrain or non-centrally available takeoff locations. (Table 3; as a supplement, I think; Columns: Site, forest,
 161 elevation, rep, CWD, surveyed area, survey date).

162 We preprogrammed transect paths using Map Pilot for DJI on iOS (hereafter Map Pilot) (Easy 2018). All
 163 transects tracked the terrain and their altitude remained approximately constant at 120 meters above ground
 164 level in order to maintain consistent ground sampling distance in the imagery. Ground level was based on a
 165 1-arc-second digital elevation model (Farr et al. 2007) and we implemented terrain following using Map Pilot.
 166 For this analysis, we dropped 4 sites whose imagery was of insufficient quality to process.

167 Structure from motion (SfM) processing requires highly overlapping images, especially in densely vegetated
 168 areas. We planned transects with 90% forward overlap and 90% side overlap at 100 meters below the lens.
 169 Thus, with flights being at 120 meters above ground level, we achieved slightly higher than 90/90 overlap for
 170 objects 20 meters tall or shorter (91.6/91.6 overlap at the ground). Overlap values were based on focal length

171 (3.6mm), sensor width (6.2mm), and image dimension (4000x3000 pixels) parameters of the Zenmuse X3
172 camera. Images were captured at a constant rate of 1 image every 2 seconds for both cameras. A forward
173 overlap of 90% at 100 meters translates to a flight speed of approximately 6.45 m/s and a side overlap of 90%
174 at 100 meters translates to transects approximately 17.2 meters apart. The Rededge camera has a different
175 focal length (5.4mm), sensor width (4.8mm), and image dimension (1280x960 pixels), which translates to
176 image overlap of 80.7/80.7 at 100m below the lens and 83.9/83.9 at ground level. Approximately 1900 photos
177 were captured over each 40 hectare survey area for each camera.

178 **Structure from motion/Photogrammetric processing**

179 We used structure from motion (SfM), aka photogrammetry, to generate orthorectified reflectance maps,
180 digital surface models, and dense point clouds for each field site. We used Pix4Dmapper Cloud to process
181 imagery using parameters ideal for images of a densely vegetated area taken by a multispectral camera.
182 For three sites, we processed the RGB and the multispectral imagery in the same project to enhance the
183 resolution of the dense point cloud. All SfM projects resulted in a single processing “block,” indicating that
184 all images in the project were optimized and processed together.

185 **Creating canopy height models**

186 We classified each survey area’s dense point cloud into “ground” and “non-ground” points using a cloth
187 simulation filter algorithm (Zhang et al. 2016) implemented in the **lidR** (Roussel et al. 2019) package. We
188 rasterized the ground points using the **raster** package (Hijmans et al. 2019) to create a digital terrain model
189 representing the ground underneath the vegetation at 1 meter resolution. We created a canopy height model
190 by subtracting the digital terrain model from the digital surface model created in Pix4Dmapper.

191 **Tree detection**

192 We tested a total of 7 automatic tree detection algorithms and a total of 177 parameter sets on the canopy
193 height model or the dense point cloud to locate trees within each site (Table 2). We used 3 parameter sets of
194 a variable window filter implemented in **ForestTools** (Plowright 2018) including the default variable window
195 filter function in **ForestTools** as well as the “pines” and “combined” functions from Popescu and Wynne
196 (2004). We used 6 parameter sets of a local maximum filter implemented in **lidR**. We used 131 parameter
197 sets of the algorithm from Li et al. (2012), which operates on the original point cloud. These parameter
198 sets included those from Shin et al. (2018) and Jakubowski et al. (2013). We used 3 parameter sets of the
199 **watershed** algorithm implemented in **lidR**, which is a wrapper for a function in the **EBImage** package (Pau
200 et al. 2010). We used 3 parameter sets of **ptrees** (Vega et al. 2014) implemented in **lidR** (Roussel et al.

201 2019) and `lidRplugins` (Roussel 2019) and which operates on the raw point cloud, without first normalizing
 202 it to height above ground level (i.e.. subtracting the ground elevation from the dense point cloud). We used
 203 the default parameter set of the `multichm` (Eysn et al. 2015) algorithm implmented in `lidR` (Roussel et
 204 al. 2019) and `lidRplugins` (Roussel 2019). We used 30 parameter sets of the experimental algorithm `lmfx`
 205 (Roussel 2019).

Table 2: Algorithm name, number of parameter sets tested for each algorithm, and references.

Algorithm	Parameter sets tested	Reference(s)
li2012	131	Li et al. (2012); Jakubowski et al. (2013); Shin et al. (2018)
lmfx	30	Roussel (2019)
localMaxima	6	Roussel et al. (2019)
multichm	1	Eysn et al. (2015)
ptrees	3	Vega et al. (2014)
vwf	3	Plowright (2018)
watershed	3	Pau et al. (2010)

206 Map ground data

207 Each orthorectified reflectance map was inspected to locate the 5 orange “X”s marking the center of the
 208 field plots. We were able to locate 110 out of 180 field plots and were then able to use these plots for
 209 validation of automated tree detection algorithms. We used the `sf` package (Pebesma et al. 2019) to convert
 210 distance-from-center and azimuth measurements of each tree in the ground plots to an x-y position on the
 211 SfM-derived reflectance map using the x-y position of the orange X visible in the reflectance map as the
 212 center.

213 Correspondence of automatic tree detection with ground data

214 We calculated 7 forest structure metrics for each field plot using the ground data collected by Fettig et al.
 215 (2019): total number of trees, number of trees greater than 15 meters, mean height of trees, 25th percentile
 216 tree height, 75th percentile tree height, mean distance to nearest tree neighbor, mean distance to 2nd nearest
 217 neighbor.

218 For each tree detection algorithm and parameter set described above, we calculated the same set of 7 structure
219 metrics within the footprint of the validation field plots. We calculated the Pearson's correlation and root
220 mean square error (RMSE) between the ground data and the aerial data for each of the 7 structure metrics
221 for each of the 177 automatic tree detection algorithms/parameter sets.

222 For each algorithm and parameter set, we calculated its performance relative to other algorithms as whether
223 its Pearson's correlation was within 5% of the highest Pearson's correlation as well as whether its RMSE was
224 within 5% of the lowest RMSE. For each algorithm/parameter set, we summed the number of forest structure
225 metrics for which it reached these 5% thresholds. For automatically detecting trees across the whole study,
226 we selected the algorithm/parameter set that performed well across the most number of forest metrics.

227 **Segmentation of crowns**

228 We delineated individual tree crowns with a marker controlled watershed segmentation algorithm (Meyer and
229 Beucher 1990) using the detected treetops as markers implemented in the **ForestTools** package (Plowright
230 2018). If the automatic segmentation algorithm failed to generate a crown segment for a detected tree (e.g.,
231 often snags with a very small crown footprint), a circular crown was generated with a radius of 0.5 meters. If
232 the segmentation generated multiple polygons for a single detected tree, only the polygon containing the
233 detected tree was retained. Image overlap decreases near the edges of the overall flight path, which reduces
234 the quality of the SfM processing in those areas. Thus, we excluded segmented crowns within 35 meters of
235 the edge of the survey area. Given the narrower field of view of the RedEdge multispectral camera versus
236 the X3 RGB camera whose optical parameters were used to define the ~40 hectare survey area around each
237 site, as well as the 35 meter additional buffering, the survey area at each site was approximately 30 hectares
238 (Table 3).

239 We used the **velox** package (Hunziker 2017) to extract all the pixel values from the orthorectified reflectance
240 map for each of the 5 narrow bands within each segmented crown polygon. Per pixel, we additionally
241 calculated the normalized difference vegetation index (NDVI; Rouse et al. (1973)), the normalized difference
242 red edge (NDRE; Gitelson and Merzlyak (1994)), the red-green index (RGI; Coops et al. (2006)), the red
243 edge chlorophyll index (CI[red edge]; Clevers and Gitelson (2013)), and the green chlorophyll index (CI[green];
244 Clevers and Gitelson (2013)). For each crown polygon, we calculated the mean value for each raw and derived
245 reflectance band (5 raw; 5 derived).

246 **Classification of trees**

247 We overlaid the segmented crowns on the reflectance maps from 20 sites spanning the latitudinal and
248 elevational gradient in the study. Using QGIS, we hand classified 564 trees as live/dead and as one of 5
249 dominant species in the study area (*Pinus ponderosa*, *Pinus lambertiana*, *Abies concolor*, *Calocedrus decurrens*,
250 or *Quercus kelloggii*) using the mapped ground data as a guide.

251 We used all 10 mean values of the reflectance bands for each tree crown polygon to predict whether the hand
252 classified trees were alive or dead using a boosted logistic regression model implemented in the **caret** package
253 (accuracy of live/dead classification on a withheld test dataset: 97.3%) (Kuhn 2008). For just the living trees,
254 we similarly used all 10 reflectance values to predict the tree species using regularized discriminant analysis
255 implemented in the **caret** package (accuracy of species classification on a withheld testing dataset: 66.7%;
256 accuracy of WPB host/non-WPB-host (i.e., ponderosa pine versus other tree species) on a withheld testing
257 dataset: 74.4%).

258 Finally, we used these models to classify all tree crowns in the data set as alive or dead as well as the species
259 of living trees.

260 **Allometric scaling of height to basal area**

261 We converted the height of each tree determined using the canopy height model to its basal area. Using
262 the tree height and diameter at breast height (DBH; breast height = 1.37m) ground data from Fettig et al.
263 (2019), we fit a simple linear regression to predict DBH from height for each of the 5 dominant species. Using
264 the model-classified tree species of each segmented tree, we used the corresponding linear relationship for
265 that species to estimate the DBH given the tree's height. We then calculated each tree's basal area, assuming
266 no tapering from breast height.

267 **Note on assumptions about dead trees**

268 For the purposes of this study, we assumed that all dead trees were ponderosa pine and were thus host trees
269 for the western pine beetle. This is a reasonably good assumption, given that Fettig et al. (2019) found that
270 73.4% of the dead trees in the coincident ground plots were ponderosa pine. The species contributing to
271 the next highest proportion of dead trees was incense cedar which represented 18.72% of the dead trees in
272 the ground plots. Incense cedar is not a potential host of the western pine beetle, and we expand on the
273 limitations of this study given the assumption of dead trees being ponderosa pine in the Discussion.

274 **Rasterizing individual tree data**

275 Because the tree detection algorithms were validated against ground data at the plot level, we rasterized the
276 classified trees at a spatial resolution similar to that of the ground plots (rasterized to 20m x 20m equalling
277 400 m²; circular ground plots with 11.35m radius equalling 404 m²). In each raster cell, we calculated the:
278 number of live trees, number of dead trees, number of ponderosa pine trees, total number of trees (of all
279 species, including ponderosa pine), quadratic mean diameter (QMD) of ponderosa pine trees, and QMD of all
280 trees of any species (overall QMD). We converted the count of ponderosa pine trees and the total tree count
281 to a density measurement of trees per hectare (tpha) by multiplying the counts in each 20m x 20m cell by 25
282 to create a “host density” and an “overall density” variable per cell.

283 **Environmental data**

284 We used climatic water deficit (CWD) (Stephenson 1998) from the 1981-2010 mean value of the basin
285 characterization model (Flint et al. 2013) as an integrated measure of temperature and moisture conditions
286 for each cell. Higher values of CWD correspond to hotter, drier conditions and lower values correspond
287 to cooler, wetter conditions CWD has been shown to correlate well with broad patterns of tree mortality
288 in the Sierra Nevada (Young et al. 2017). We resampled the climatic water deficit product using bilinear
289 interpolation implemented in the `raster` package to match the 20m x 20m spatial scale of the other variables.
290 We converted the CWD value for each cell into a z-score representing that cell’s deviation from the mean
291 CWD across the climatic range of Sierra Nevada ponderosa pine as determined from 179 herbarium records
292 described in Baldwin et al. (2017). Thus, a CWD z-score of one would indicate that the CWD at that
293 cell is one standard deviation hotter/drier than the mean CWD across all geolocated herbarium records for
294 ponderosa pine in the Sierra Nevada.

295 **Statistical model**

296 We used a generalized linear model with a zero-inflated binomial response and a logit link to predict the
297 probability of ponderosa pine mortality within each raster cell as a function of the crossed effects of ponderosa
298 pine quadratic mean diameter and density added to the crossed effect of overall quadratic mean diameter and
299 density as well as the interaction of each summand with climatic water deficit at each site.
300 To measure and account for spatial autocorrelation of the bark beetle behavioral processes underlying
301 ponderosa mortality, we first subsampled the data at each site to a random selection of 200, 20m x 20m
302 cells representing approximately 27.5% of the surveyed area. With these subsampled data, we included a
303 separate exact Gaussian process term per site of the interaction between the x- and y-position of each cell

304 using the `gp()` function in the `brms` package (Bürkner 2017). The Gaussian process accounts for spatial
 305 autocorrelation in the model by jointly estimating the spatial covariance of the response variable with the
 306 effects of the other covariates.

$$y_{i,j} \sim \begin{cases} 0, & p \\ Binom(n_i, \pi_i), & 1 - p \end{cases}$$

$$\text{logit}(\pi_i) = \beta_0 +$$

$$\beta_1 X_{cwd,j} +$$

$$\beta_1 X_{cwd,j} (\beta_2 X_{\text{pip}oQMD,i} + \beta_3 X_{\text{pip}o\text{Density},i} + \beta_4 X_{\text{pip}oQMD,i} X_{\text{pip}o\text{Density},i}) +$$

$$\beta_1 X_{cwd,j} (\beta_5 X_{\text{overall}QMD,i} + \beta_6 X_{\text{overall}\text{Density},i} + \beta_7 X_{\text{overall}QMD,i} X_{\text{overall}\text{Density},i}) +$$

$$\mathcal{GP}_j(x_i, y_i)$$

307 Where y_i is the number of dead trees in cell i , n_i is the sum of the dead trees and live ponderosa pine trees
 308 in cell i , π_i is the probability of ponderosa pine tree mortality in cell i , p is the probability of there being
 309 zero dead trees in a cell arising as a result of an unmodeled process, $X_{cwd,j}$ is the z-score of climatic water
 310 deficit for site j , $X_{\text{pip}oQMD,i}$ is the scaled quadratic mean diameter of ponderosa pine in cell i , $X_{\text{pip}o\text{Density},i}$
 311 is the scaled density of ponderosa pine trees in cell i , $X_{\text{overall}QMD,i}$ is the scaled quadratic mean diameter
 312 of all trees in cell i , $X_{\text{overall}\text{Density},i}$ is the scaled density of all trees in cell i , x_i and y_i are the x- and y-
 313 coordinates of the centroid of the cell in an EPSG3310 coordinate reference system, and \mathcal{GP}_j represents the
 314 exact Gaussian process describing the spatial covariance between cells at site j .

315 We used 4 chains with 2000 iterations each (1000 warmup, 1000 samples), and confirmed chain convergence
 316 by ensuring all `Rhat` values were less than 1.1 (Brooks and Gelman 1998). We used posterior predictive
 317 checks to visually confirm model performance by overlaying the density curves of the predicted number of
 318 dead trees per cell over the observed number (Gabry et al. 2019). For the posterior predictive checks, we
 319 used 50 random samples from the model fit to generate 50 density curves and ensured curves were centered
 320 on the observed distribution, paying special attention to model performance at capturing counts of zero.

321 Software and data availability

322 All data are available via the Open Science Framework. Statistical analyses were performed using the `brms`
 323 packages. With the exception of the SfM software (Pix4Dmapper Cloud) and the GIS software QGIS, all
 324 data carpentry and analyses were performed using R (R Core Team 2018).

325 **Results**

Table 3: Site characteristics for each of the 32 sites. The site name consists of the forest name, elevation band, and rep separated by an underscore. The Eldorado National Forest is ‘eldo’, the Stanislaus National Forest is ‘stan’, the Sierra National Forest is ‘sier’, and the Sequoia National Forest is ‘sequ’. The elevation band represents the lower bounds of the 305 meter (1000 foot) elevation bands in feet. Thus ‘3k’ implies that site was located between 3,000 and 4,000 feet (914-1219 meters). Aerially detected mortality and density of the whole site is presented along with the mortality and density calculated from the ground data (aerial / ground). The density is measured in trees per hectare (tpha).

Site	CWD (mm)	CWD (z-score)	Survey area (ha)	Mortality (aerial/ground)	Density (tpha; aerial/ground)
eldo_3k_1	678	0.319	31.02	0.11/0.61	630.01/410.19
eldo_3k_2	706	0.501	30.61	0.12/0.36	444.26/647.42
eldo_3k_3	655	0.163	30.95	0.22/0.36	492.63/410.19
eldo_4k_1	570	-0.383	28.04	0.09/0.39	632.82/588.11
eldo_4k_2	642	0.0831	28.41	0.15/0.78	338.20/271.82
eldo_5k_1	663	0.219	28.44	0.11/0.44	661.80/543.63
eldo_5k_2	627	-0.0132	30.02	0.12/0.36	584.89/968.65
eldo_5k_3	599	-0.2	29.73	0.07/0.32	488.66/622.71
stan_3k_1	638	0.059	31.04	0.10/0.52	739.45/1037.84
stan_3k_2	739	0.713	18.78	0.40/0.78	433.53/405.25
stan_3k_3	762	0.859	30.1	0.22/0.41	558.43/326.18
stan_4k_1	540	-0.58	29.62	0.29/0.63	507.61/711.66
stan_4k_2	528	-0.658	30.54	0.18/0.56	481.85/256.99
stan_5k_1	524	-0.688	30.94	0.19/0.54	388.89/336.06
stan_5k_2	524	-0.685	29.94	0.21/0.44	399.33/622.71
sier_3k_1	764	0.871	30.42	0.19/0.48	651.46/850.04
sier_3k_2	768	0.898	30.05	0.20/0.77	438.84/153.21

Site	CWD (mm)	CWD (z-score)	Survey area (ha)	Mortality (aerial/ground)	Density (tpha; aerial/ground)
sier_3k_3	773	0.932	29.77	0.32/0.77	511.26/459.62
sier_4k_1	841	1.38	30.43	0.54/0.51	576.15/538.69
sier_4k_2	764	0.877	29.3	0.33/0.57	499.43/854.98
sier_4k_3	688	0.383	26.39	0.48/0.59	454.23/499.15
sier_5k_1	722	0.599	14.59	0.41/0.43	631.30/716.60
sier_5k_2	710	0.523	27.53	0.53/0.74	477.29/454.67
sier_5k_3	779	0.968	28.93	0.33/0.43	569.44/484.33
sequ_4k_1	767	0.891	29.59	0.50/0.56	365.81/607.88
sequ_4k_3	816	1.21	29.69	0.35/0.71	433.35/306.41
sequ_5k_1	718	0.577	27.12	0.35/0.52	364.01/444.79
sequ_5k_2	587	-0.274	29.1	0.45/0.43	478.31/499.15
sequ_5k_3	611	-0.117	31.34	0.42/0.48	348.68/494.21
sequ_6k_1	731	0.657	27.78	0.30/0.70	433.43/360.77
sequ_6k_2	690	0.39	11.83	0.26/0.43	699.04/934.06
sequ_6k_3	603	-0.174	26.51	0.36/0.32	535.54/691.89

326 **Tree detection**

327 We found that the experimental `lmfx` algorithm with parameter values of `dist2d = 1` and `ws = 2.5` (Roussel
 328 et al. 2019) performed the best across 7 measures of forest structure as measured by Pearson's correlation
 329 with ground data (Table 3).

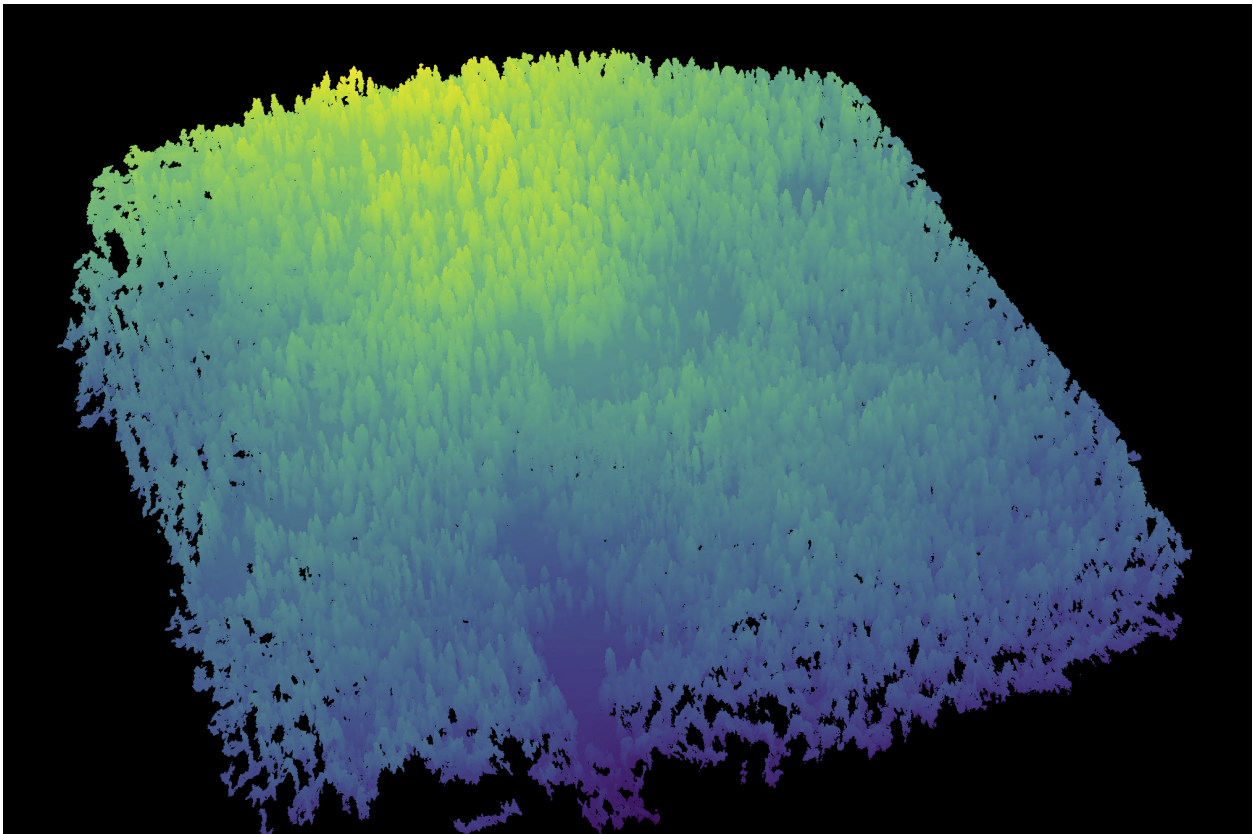


Figure 2: A dense point cloud representing ~40 hectares of forest is generated using Structure from Motion (SfM) processing of ~1900 images. The dense point cloud z- position represents the ground elevation plus the vegetation height.

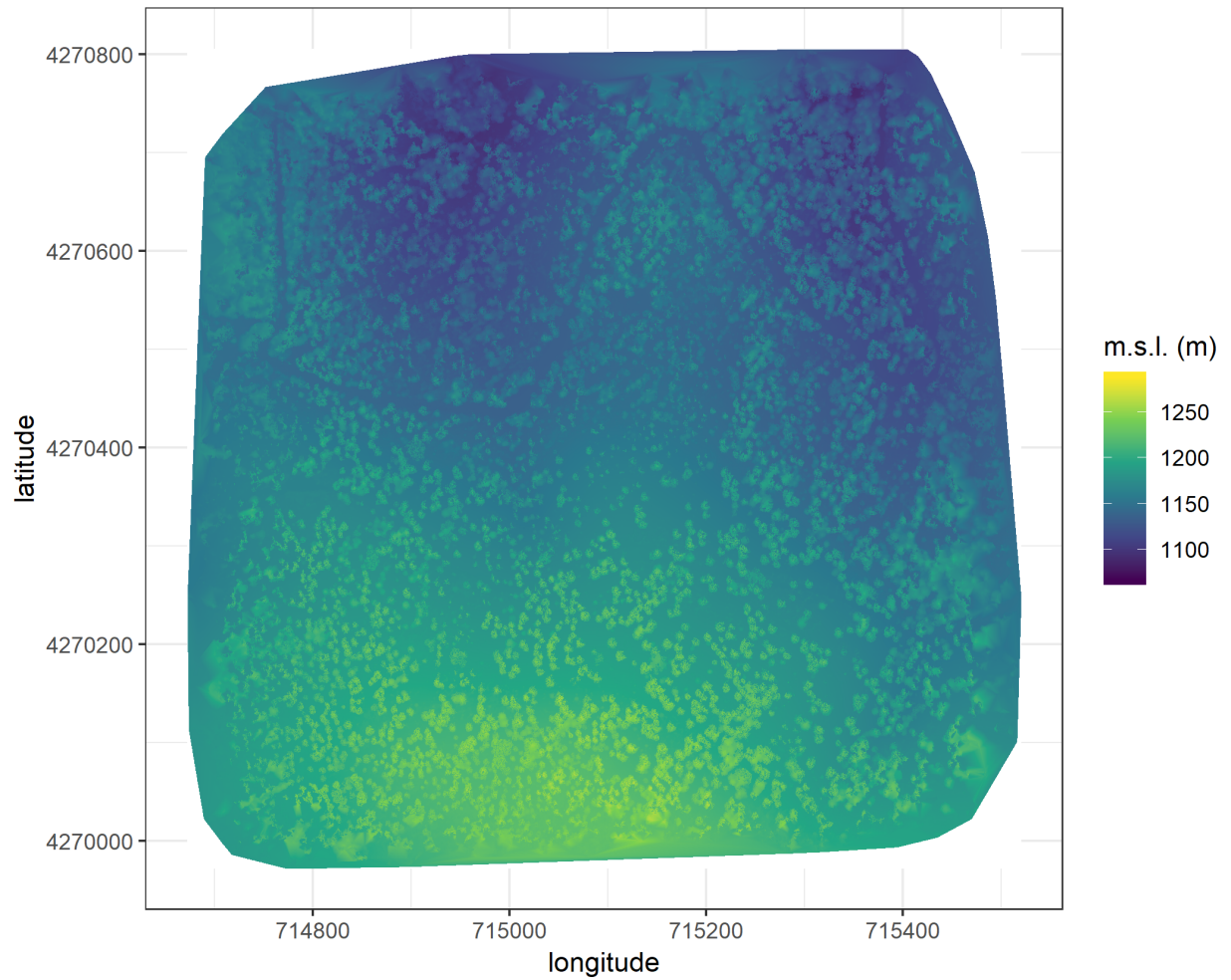


Figure 3: The digital surface model (DSM) is a 2-dimensional representation of the dense point cloud generated using structure from motion (SfM) processing. The DSM represents the ground elevation plus the vegetation height.

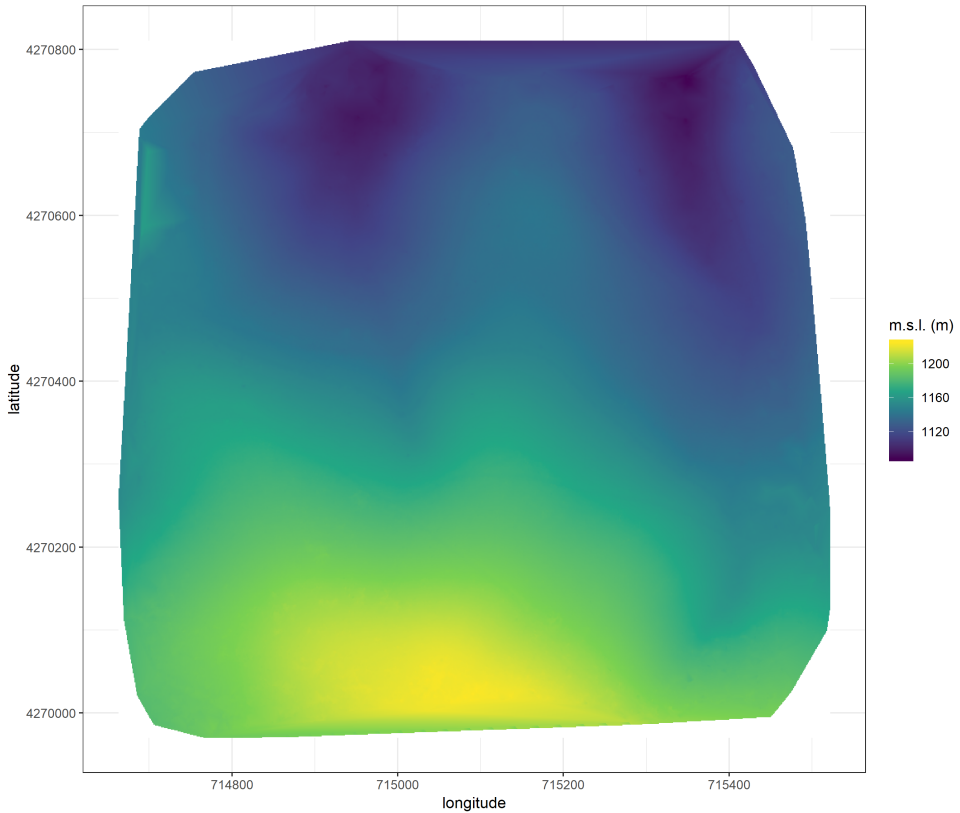


Figure 4: The digital terrain model (DTM) is generated by processing the dense point cloud using the cloth simulation filter algorithm (Zhang et al. 2016), which classifies points as “ground” or “not-ground” and then interpolates the “ground” elevation using Delaunay triangulation for the rest of the dense point cloud footprint. The DTM represents the ground elevation without any vegetation.

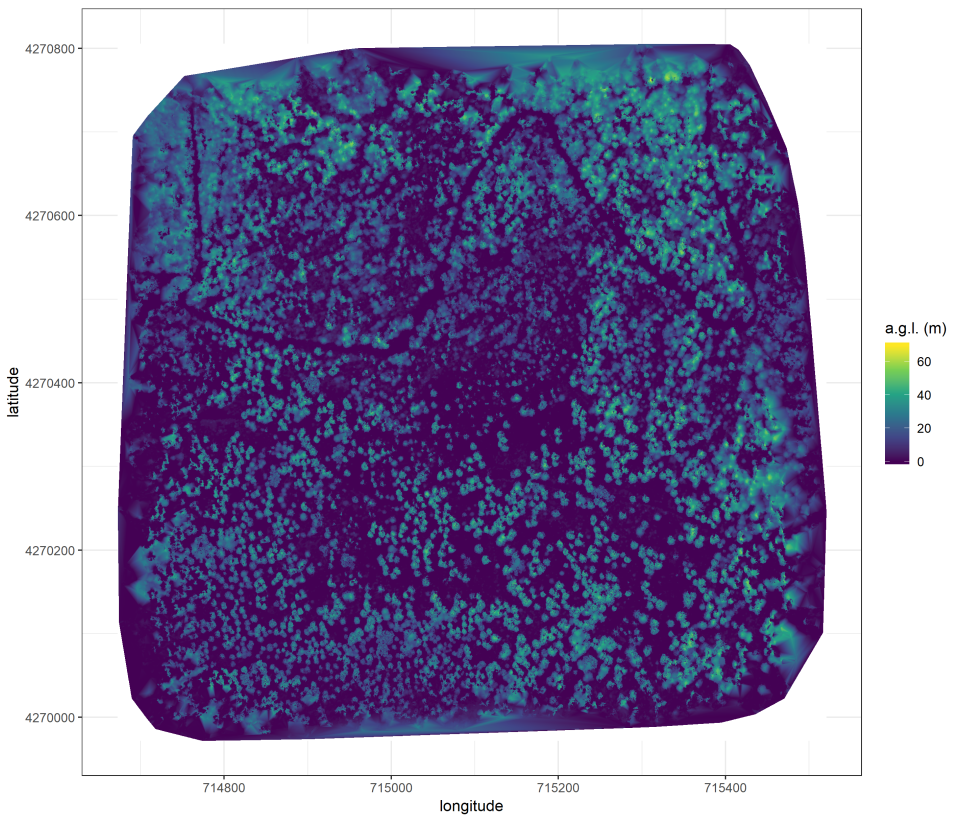


Figure 5: The canopy height model (CHM) is generated by subtracting the digital terrain model from the digital surface model. The CHM represents the height of all of the elevation above ground level.

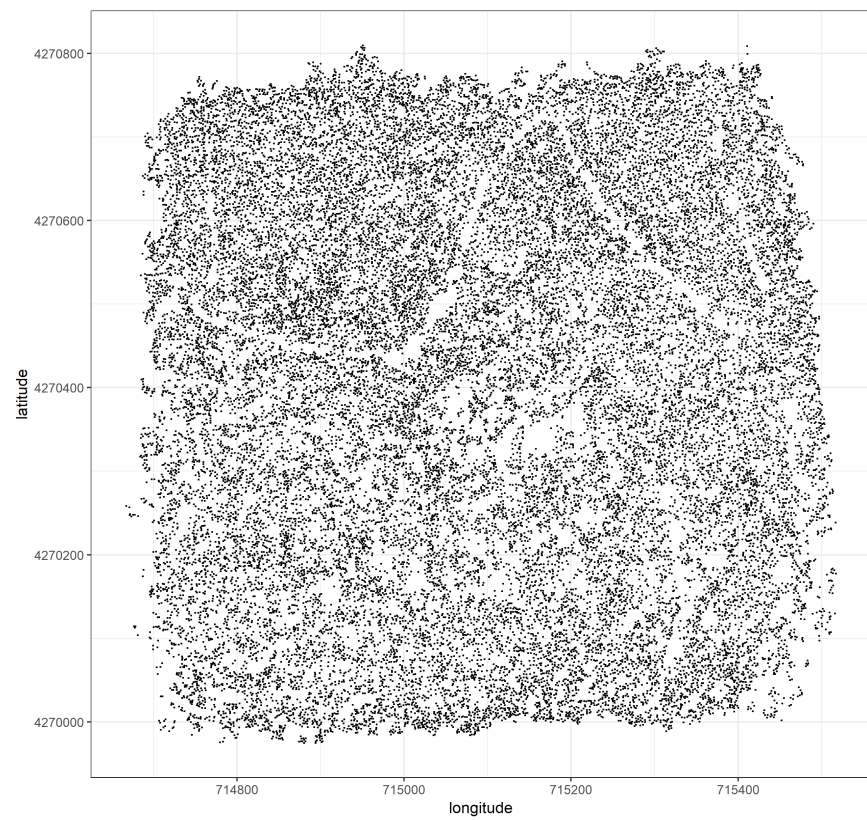


Figure 6: Tree locations are detected using the `lmfx` (Roussel et al. 2019) treetop detection algorithm on the dense point cloud.

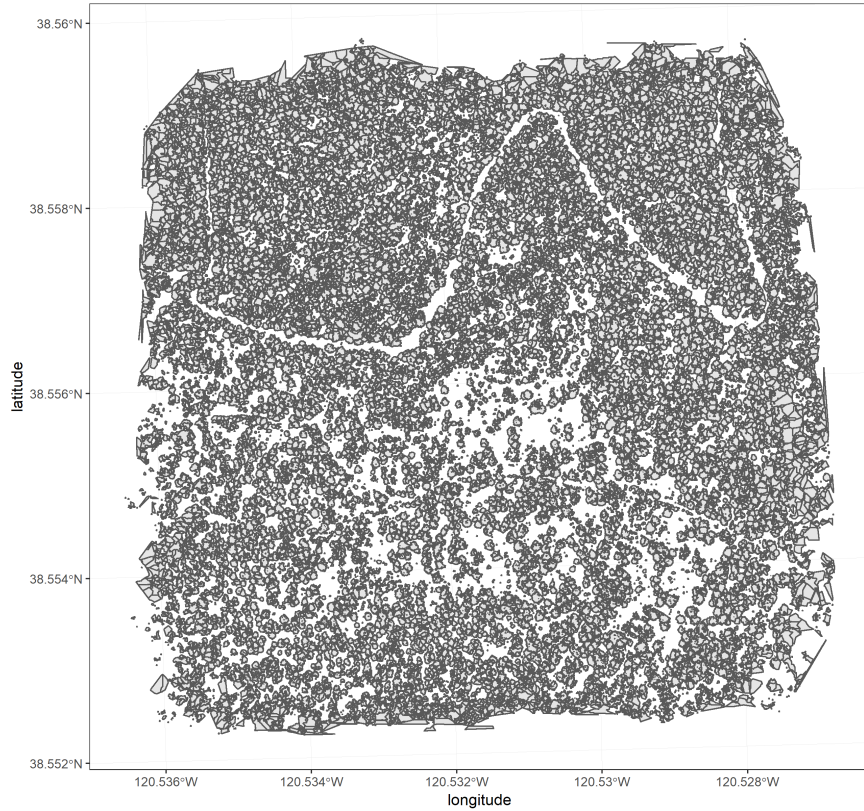


Figure 7: Individual crowns are delineated using a marker controlled watershed segmentation algorithm (Meyer and Beucher 1990, Plowright 2018) on the canopy height model (CHM) using the detected tree locations as a priority map. If the algorithm failed to delineate a crown for a tree that was identified in the tree detection step, a circular crown with a 0.5m buffer centered on point location of the detected tree was added as a crown.

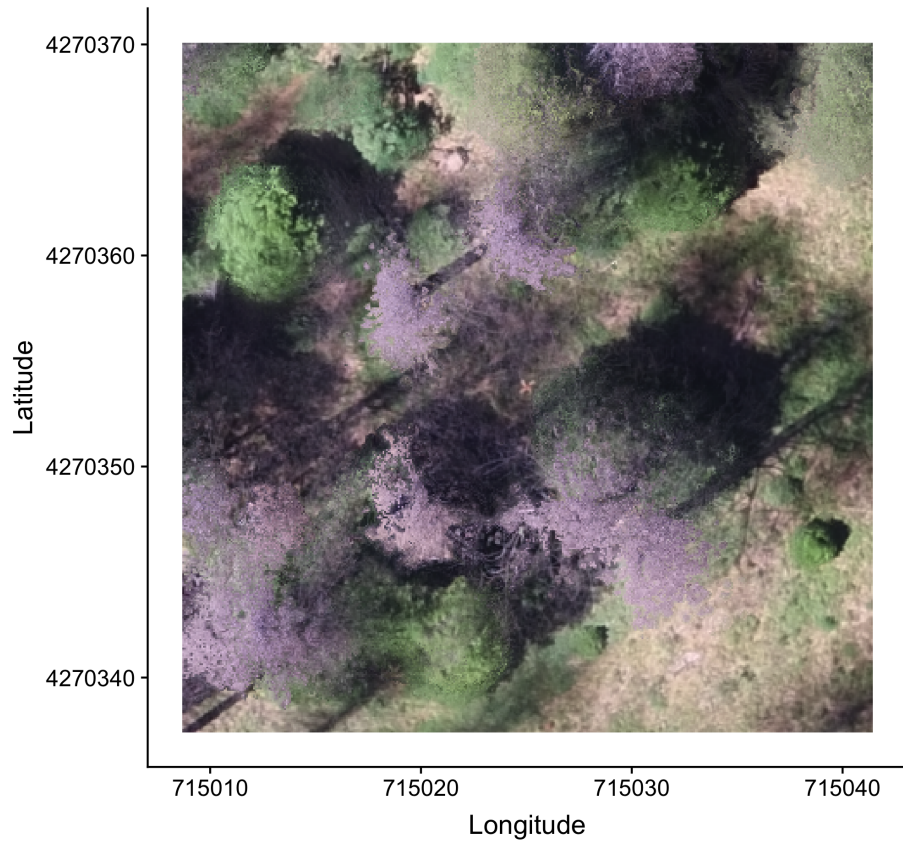


Figure 8: The orthomosaic for each of the 32 sites is generated with the Structure from Motion (SfM) processing, showing a top-down view of the whole survey area such that distances between objects in the scene are preserved and can be measured. Depicted is an example orthomosaic for one of the 32 sites cropped to the extent of a single ground plot (5 ground plots per site) showing the orange X placed at exactly the plot center prior to flight. The original orthomosaic for the whole site represents an area approximately 1000 times as large as the area depicted here.

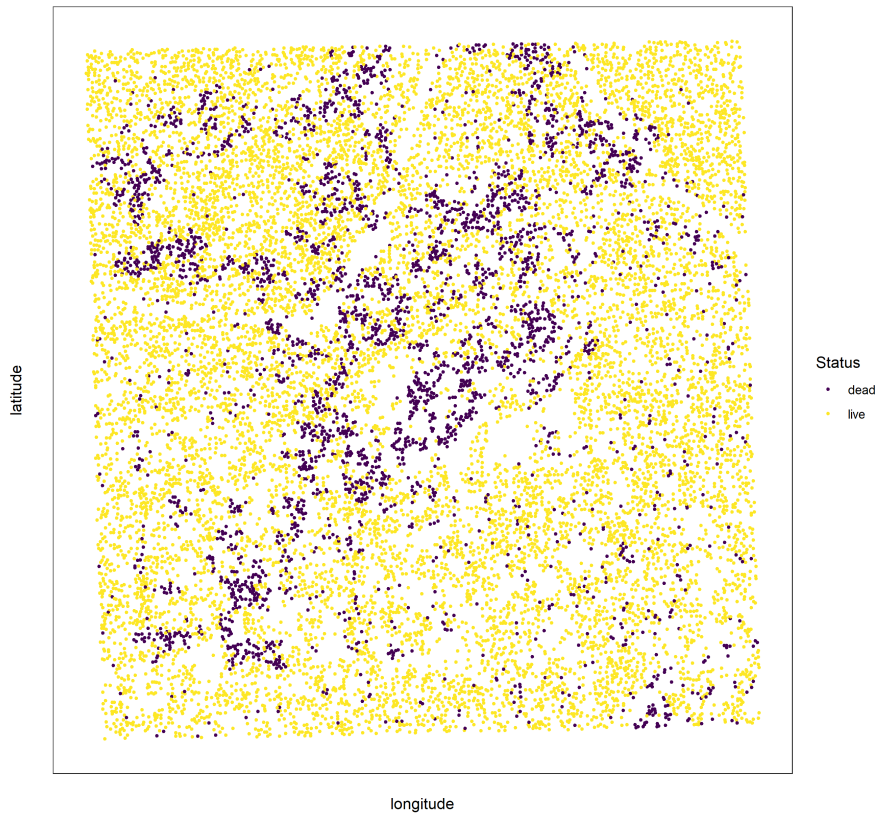


Figure 9: Each tree is classified as live or dead by extracting the pixel values from the 5 narrow bands of the Rededge3 camera (and 5 derived bands– see methods) in the orthomosaic within each segmented tree crown of the detected trees, taking their mean value, and using those means to predict live/dead status with a boosted logistic regression previously trained on a hand-classified set of segmented crowns from across the study area.

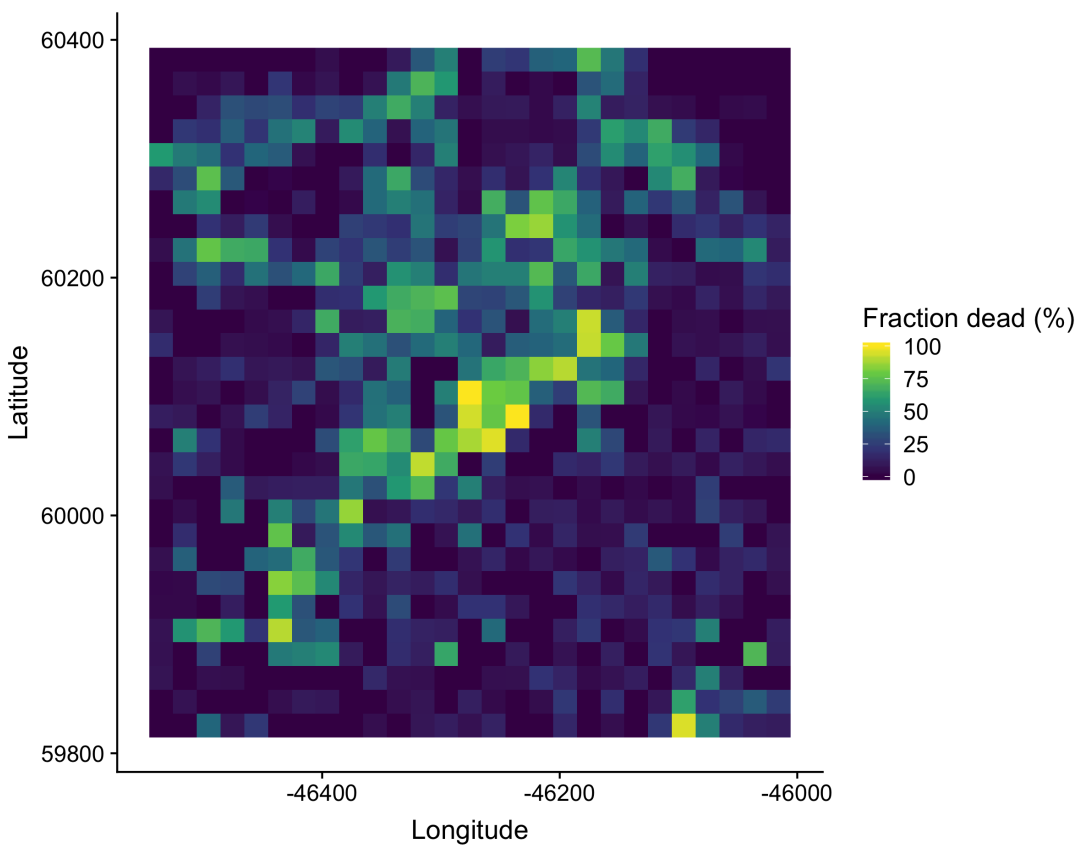


Figure 10: We rasterized the individual tree data by aggregating values to 20m x 20m cells. This example shows the proportion of dead trees per cell for the same example site as in the previous figures.

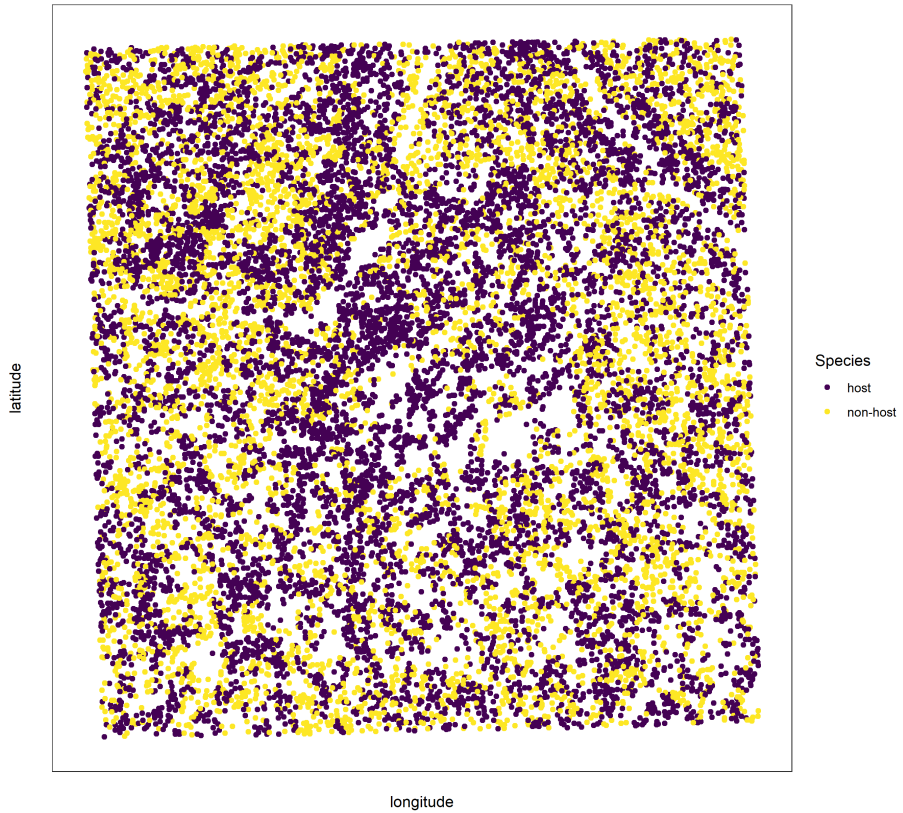


Figure 11: For each live tree, we classified its species using the same means of extracted pixel values across the 5 Rededge3 narrow bands (and 5 derived bands) as predictors in a regularized discriminant analysis previously trained on a hand-classified set of segmented crowns from across the study area. Host/non-host data were also rasterized as in the previous figure prior to analyses (not shown).

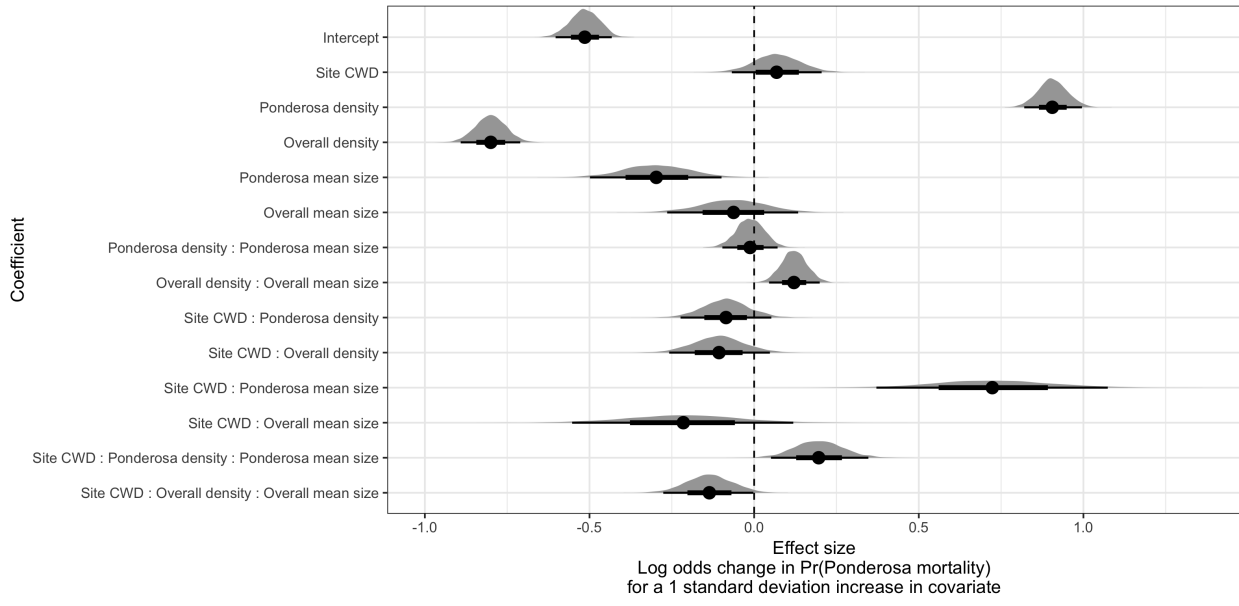


Figure 12: Posterior distributions of effect size from zero-inflated binomial model predicting the probability of ponderosa pine mortality in a 20m x 20m cell given forest structure characteristics of host trees and all trees within the cell, as well as a site-level climatic water deficit. The gray density distribution for each model covariate represents the density of the posterior distribution, the point underneath each density curve represents the median of the estimate, the bold interval surrounding the point estimate represents the 66% credible interval, and the thin interval surrounding the point estimate represents the 95% credible interval.

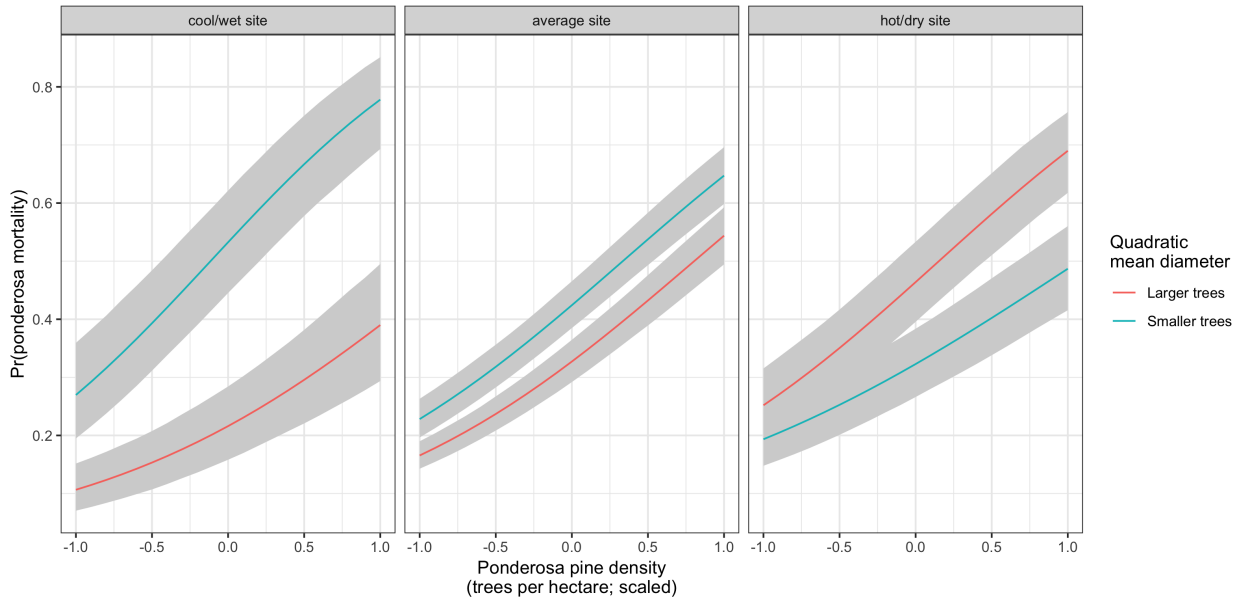


Figure 13: Line version of model results with 95% credible intervals showing primary influence of ponderosa pine structure on the probability of ponderosa pine mortality, and the interaction across climatic water deficit. The “larger trees” line represents the quadratic mean diameter of ponderosa pine 0.7 standard deviations above the mean, and the “smaller trees” line represents the quadratic mean diameter of ponderosa pine 0.7 standard deviations below the mean.

Table 4: Correlation and differences between the best performing tree detection algorithm (lmfx with dist2d = 1 and ws = 2.5) and the ground data. An asterisk next to the correlation or RMSE indicates that this value was within 5% of the value of the best-performing algorithm/parameter set. Ground mean represents the mean value of the forest metric across the 110 ground plots that were visible from the sUAS-derived imagery. The median error is calculated as the median of the differences between the air and ground values for the 110 visible plots. Thus, a positive number indicates an overestimate by the sUAS workflow and a negative number indicates an underestimate.

Forest structure metric	Ground mean	Correlation with ground	RMSE	Median error
total tree count	19	0.67*	8.68*	2
count of trees > 15m	9.9	0.43	7.38	0
dist to 1st nearest neighbor	2.8	0.55*	1.16*	0.26
(m)				
dist to 2nd nearest neighbor	4.3	0.61*	1.70*	0.12
(m)				
height (m); 25th percentile	12	0.16	8.46	-1.2
height (m); mean	18	0.29	7.81*	-2.3
height (m); 75th percentile	25	0.35	10.33*	-4

330 Effect of local structure and regional climate on western pine beetle severity

331 We detected no main effect of climatic water deficit on the probability of ponderosa pine mortality within
332 each 20m x 20m cell.

333 We found a strong main effect of ponderosa pine local density, accounting for quadratic mean diameter of
334 ponderosa pine, with greater density increasing the probability of ponderosa pine mortality.

335 Conversely, we found a generally negative effect of quadratic mean diameter of ponderosa pine on the
336 probability of ponderosa mortality, suggesting that the western pine beetle attacked smaller trees, on average.

337 There was a strong positive interaction between the climatic water deficit and ponderosa pine quadratic mean

338 diameter, such that larger trees were more likely to increase the probability of ponderosa mortality in hotter,
339 drier sites.

340 We found negative main effects of overall tree density and overall quadratic mean diameter. There was a
341 positive interaction between these variables, such that denser stands with larger trees did lead to greater
342 ponderosa pine mortality.

343 **Spatial effects**

344 We were able to calculate the length scale of the spatial autocorrelation in the probability of ponderosa
345 pine mortality at each site, accounting for forest structure and environmental factors. By fitting a separate
346 approximate Gaussian process for each site on the interacting variables of the x- and y- position, we measured
347 the spatial covariance inherent in the data, accounting for other factors.

348 **Discussion**

349 Climate change adaptation strategies emphasize reducing tree densities (North et al. 2015, Young et al.
350 2017), but understanding the optimal scale and pattern of tree distributions that can mitigate bark beetle
351 outbreaks will be vital for predicting how California forests may respond to these interventions.

352 that rapidly emerge over weeks to months but have long-lasting effects on forest conditions.

353 and limit insights into phenomena like the recent bark beetle disturbance in Sierra yellow pine/mixed-conifer
354 forests.

355 **Closer spacing between potential host trees facilitates dispersal**

356 If this drives mortality patterns, then we'd expect the local density of ponderosa pine trees, accounting for
357 other variables, to have a strong positive effect.

358 **Host preference for large trees**

359 If this drives mortality patterns, then we'd expect the quadratic mean diameter of ponderosa pine trees,
360 accounting for other variables, to have a strong positive effect.

361 **Denser forests augment pheromone communication**

362 If this drives mortality patterns, then we'd expect the local density of all trees, accounting for other variables,
363 to have a strong positive effect.

364 **Tree crowding leads to greater average water stress per tree**

365 If this drives mortality patterns, then we'd expect the quadratic mean diameter of all trees, accounting for
366 other factors, to have a strong positive effect.

367 **Interaction between host density and host size**

368 A positive coefficient would indicate a combined effect of WPB preference for large trees and nearby host
369 availability.

370 **Interaction between all tree density and all tree size**

371 A positive coefficient would indicate a combined effect of tree crowding and pheromone communication
372 enhancement.

373 **Implications of forest structure/regional climate interactions**

374 We found that the probability of ponderosa pine mortality generally increased with local host availability
375 (host density), but also interacted with both host size and regional climate such that the role of tree size
376 became increasingly important in more climatically extreme sites. A smaller average tree size led to a lower
377 probability of ponderosa mortality in cool/wet sites and a larger average tree size led to a greater probability
378 of ponderosa mortality in hot/dry sites. These mortality patterns highlight a possible distinction in behavior
379 between the recent western bark beetle activity across the gradient of climatic water deficit. Even in the most
380 highly impacted forest stands (because our study sites were selected conditional on there being high levels of
381 western pine beetle activity), there is still a detectable effect of tree size such that the smaller (presumably
382 weaker) trees are getting killed in cooler/wetter sites, and the larger (presumably more well-defended) trees
383 are getting killed more in the hotter/drier sites. So while mortality is high everywhere, there does appear to
384 be a difference in the beetle choosiness across the climatic water deficit gradient.

385 **Similarities and differences with Fettig et al. (2019)**

386 Fettig et al. (2019) found positive relationship between number of trees killed and: total number of trees,
387 total basal area, stand density index.

388 Fettig et al. (2019) found negative relationship between the proportion of trees killed and: total number of
389 trees, stand density index.

390 Host availability and suitability are usually considered the major factors affecting beetle population behavior
391 (Reid 1963; Berryman 1973, 1976, 1978a, 1982a; Cole 1981; Amman 1984). (Raffa and Berryman 1987)

392 Hayes et al. (2009) and Fettig et al. (2019) found measures of host availability explained less variation in
393 mortality than measures of stand density.

394 Negrón et al. (2009) reported positive association of probability of ponderosa pine mortality and tree density
395 during a drought in Arizona.

396 Effect of competition may be masked because drought was so extreme Fettig et al. (2019); Floyd et al.
397 (2009), which is perhaps why we saw a counter-intuitive signal of increasing total basal area leading to lower
398 probability of ponderosa pine mortality.

399 **Broader context around field plots**

400 We surveyed 9 square kilometers of forest representing ~450,000 trees along a broad environmental gradient
401 of climatic water deficit. Site selection and small plot size can influence inference. For instance, Fettig et
402 al. (2019) reported statistically undetectable differences in overall mortality in their plot network across 4
403 national forests. By expanding the hectarage surveyed by a factor of 200, we detected dramatic differences in
404 overall mortality.

405 This is about more than sample size (though that helps). This is also about capturing the local disturbance
406 phenomenon.

407 **Implications for future forest structure**

408 We have demonstrated that forest structure (local host density and size) affected the cumulative severity
409 of the western pine beetle in the Sierra Nevada in the 2012 to 2015 drought and its aftermath. Clearly,
410 this forest insect disturbance has reciprically impacted the forest structure, with uncertain consequences for
411 long-term forest dynamics.

412 Small trees are getting killed in cooler/wetter sites, larger trees getting killed in hotter/drier sites. Perhaps
413 the cooler/wetter sites are resisting even this massive disturbance event?

414 **Spatial effect**

415 The western pine beetle is known to exhibit strong aggregation and anti-aggregation behavior arising from
416 its pheromone communication, and thus it is likely that the measured spatial covariance in this study is
417 attributable in part to the magnitude of this effect at each site.

418 Some studies have suggested that “outbreak” conditions are distinguishable by clustered tree mortality, but
419 this is perhaps challenging to tease apart (Raffa et al. 2008). Our modeling framework allows for a joint

420 estimation of the effects of forest structure, environmental condition, and the spatial effect. This framework
421 would be enhanced with confidence in individual tree level data, and a lot of it, along with a strong gradient
422 of environmental conditions and forest structure.

423 We won't interpret this measure of contagion, because the uncertainties in this particular study are too great
424 (tree detection, species classification, dead trees all assumed to be WPB hosts, didn't account for topographic
425 effects which could also manifest as part of this spatial covariance process). We do suggest that this could be
426 a meaningful and quantifiable means of assessing bark beetle "stage of outbreak".

427 **Future spatial directions (will cut this; here for now so I can write it down elsewhere)**

428 Perhaps could also compare relative effect of individual tree spacing (Voronoi polygon area) with the length
429 scale parameter at a certain site to get at a similar question. A big voronoi polygon area effect and a short
430 covariance kernel tells us that it's a water stress effect– a crowded tree gets attacked regardless of whether
431 nearby trees were attacked. A small voronoi polygon area effect and a long covariance kernel tells us that the
432 mortality is patterned more based on there being spillover from nearby attacked neighbors instead of how
433 crowded any given tree is. I expect we might see different relative magnitudes of voronoi polygon area and
434 covariance kerel effects depending on CWD.

435 **Important considerations**

436 Cumulative effect of elevated insect activity, as mortality was spread out over 5 years and we surveyed at the
437 end. All the detected dead trees were considered ponderosa pine– we know this is wrong. Only about 3 out
438 of 4 dead trees in Fettig et al. (2019) were ponderosa.

439 **Room for improvement**

- 440 • Better geometry by using higher overlap, more spatially resolved images.
- 441 • Better image classification and scalability by using instrumentation having spectral overlap with more
442 widely deployed instrumentation (e.g., Landsat).
- 443 • Better tree detection using machine learning approaches
- 444 • Our live/dead classifier works pretty well.
- 445 • Our species classifier could improve. Perhaps also using machine learning approaches.

446 (Preisler et al. 2017)

447 **References**

- 448 Asner, G. P., P. G. Brodrick, C. B. Anderson, N. Vaughn, D. E. Knapp, and R. E. Martin. 2016. Progressive
449 forest canopy water loss during the 20122015 California drought. *Proceedings of the National Academy of
450 Sciences* 113:E249–E255.
- 451 Baldwin, B. G., A. H. Thornhill, W. A. Freyman, D. D. Ackerly, M. M. Kling, N. Morueta-Holme, and B. D.
452 Mishler. 2017. Species richness and endemism in the native flora of California. *American Journal of Botany*
453 104:487–501.
- 454 Bentz, B. J., J. Régnière, C. J. Fettig, E. M. Hansen, J. L. Hayes, J. A. Hicke, R. G. Kelsey, J. F. Negrón,
455 and S. J. Seybold. 2010. Climate Change and Bark Beetles of the Western United States and Canada: Direct
456 and Indirect Effects. *BioScience* 60:602–613.
- 457 Berryman, A. A. 1982. Population dynamics of bark beetles. Pages 264–314 in *Bark Beetles in North
458 American Conifers: A System for the Study of Evolutionary Biology*.
- 459 Brooks, S. P., and A. Gelman. 1998. General Methods for Monitoring Convergence of Iterative Simulations.
460 *Journal of Computational and Graphical Statistics* 7:434.
- 461 Bürkner, P.-C. 2017. **Brms** : An *R* Package for Bayesian Multilevel Models Using *Stan*. *Journal of Statistical
462 Software* 80.
- 463 Chubaty, A. M., B. D. Roitberg, and C. Li. 2009. A dynamic host selection model for mountain pine beetle,
464 *Dendroctonus ponderosae* Hopkins. *Ecological Modelling* 220:1241–1250.
- 465 Clevers, J., and A. Gitelson. 2013. Remote estimation of crop and grass chlorophyll and nitrogen content using
466 red-edge bands on Sentinel-2 and -3. *International Journal of Applied Earth Observation and Geoinformation*
467 23:344–351.
- 468 Coops, N. C., M. Johnson, M. A. Wulder, and J. C. White. 2006. Assessment of QuickBird high spatial
469 resolution imagery to detect red attack damage due to mountain pine beetle infestation. *Remote Sensing of
470 Environment* 103:67–80.
- 471 DJI. 2015a. Zenmuse X3 - Creativity Unleashed. <https://www.dji.com/zenmuse-x3/info>.
- 472 DJI. 2015b. DJI - The World Leader in Camera Drones/Quadcopters for Aerial Photography. <https://www.dji.com/matrice100/info>.
- 473
- 474 Easy, D. M. 2018. Map Pilot for DJI. <https://itunes.apple.com/us/app/map-pilot-for-dji/id1014765000?mt=8>.
- 475 Evenden, M. L., C. M. Whitehouse, and J. Sykes. 2014. Factors Influencing Flight Capacity of the Mountain

- 476 Pine Beetle (Coleoptera: Curculionidae: Scolytinae). Environmental Entomology 43:187–196.
- 477 Eysn, L., M. Hollaus, E. Lindberg, F. Berger, J.-M. Monnet, M. Dalponte, M. Kobal, M. Pellegrini, E.
478 Lingua, D. Mongus, and N. Pfeifer. 2015. A Benchmark of Lidar-Based Single Tree Detection Methods Using
479 Heterogeneous Forest Data from the Alpine Space. Forests 6:1721–1747.
- 480 Farr, T. G., P. A. Rosen, E. Caro, R. Crippen, R. Duren, S. Hensley, M. Kobrick, M. Paller, E. Rodriguez, L.
481 Roth, D. Seal, S. Shaffer, J. Shimada, J. Umland, M. Werner, M. Oskin, D. Burbank, and D. Alsdorf. 2007.
482 The Shuttle Radar Topography Mission. Reviews of Geophysics 45.
- 483 Fettig, C. J. 2012. Chapter 2: Forest health and bark beetles. *in* Managing Sierra Nevada Forests. PSW-
484 GTR-237. USDA Forest Service.
- 485 Fettig, C. J., K. D. Klepzig, R. F. Billings, A. S. Munson, T. E. Nebeker, J. F. Negrón, and J. T. Nowak. 2007.
486 The effectiveness of vegetation management practices for prevention and control of bark beetle infestations in
487 coniferous forests of the western and southern United States. Forest Ecology and Management 238:24–53.
- 488 Fettig, C. J., L. A. Mortenson, B. M. Bulaon, and P. B. Foulk. 2019. Tree mortality following drought in the
489 central and southern Sierra Nevada, California, U.S. Forest Ecology and Management 432:164–178.
- 490 Flint, L. E., A. L. Flint, J. H. Thorne, and R. Boynton. 2013. Fine-scale hydrologic modeling for regional land-
491 scape applications: The California Basin Characterization Model development and performance. Ecological
492 Processes 2:25.
- 493 Floyd, M. L., M. Clifford, N. S. Cobb, D. Hanna, R. Delph, P. Ford, and D. Turner. 2009. Relationship of
494 stand characteristics to drought-induced mortality in three Southwestern piñonJuniper woodlands. Ecological
495 Applications 19:1223–1230.
- 496 Gabry, J., D. Simpson, A. Vehtari, M. Betancourt, and A. Gelman. 2019. Visualization in Bayesian workflow.
497 Journal of the Royal Statistical Society: Series A (Statistics in Society) 182:389–402.
- 498 Gitelson, A., and M. N. Merzlyak. 1994. Spectral Reflectance Changes Associated with Autumn Senescence
499 of Aesculus hippocastanum L. and Acer platanoides L. Leaves. Spectral Features and Relation to Chlorophyll
500 Estimation. Journal of Plant Physiology 143:286–292.
- 501 Graf, M., M. Reid, B. Aukema, and B. Lindgren. 2012. Association of tree diameter with body size and lipid
502 content of mountain pine beetles. The Canadian Entomologist 144:467–477.
- 503 Griffin, D., and K. J. Anchukaitis. 2014. How unusual is the 20122014 California drought? Geophysical

- 504 Research Letters 41:9017–9023.
- 505 Hayes, C. J., C. J. Fettig, and L. D. Merrill. 2009. Evaluation of Multiple Funnel Traps and Stand
506 Characteristics for Estimating Western Pine Beetle-Caused Tree Mortality. *Journal of Economic Entomology*
507 102:2170–2182.
- 508 Hijmans, R. J., J. van Etten, M. Sumner, J. Cheng, A. Bevan, R. Bivand, L. Busetto, M. Canty, D. Forrest,
509 A. Ghosh, D. Golicher, J. Gray, J. A. Greenberg, P. Hiemstra, I. for M. A. Geosciences, C. Karney, M.
510 Mattiuzzi, S. Mosher, J. Nowosad, E. Pebesma, O. P. Lamigueiro, E. B. Racine, B. Rowlingson, A. Shortridge,
511 B. Venables, and R. Wueest. 2019. *Raster: Geographic Data Analysis and Modeling*.
- 512 Hunziker, P. 2017. *Velox: Fast Raster Manipulation and Extraction*.
- 513 Jakubowski, M. K., W. Li, Q. Guo, and M. Kelly. 2013. Delineating Individual Trees from Lidar Data: A
514 Comparison of Vector- and Raster-based Segmentation Approaches. *Remote Sensing* 5:4163–4186.
- 515 Kane, V. R., M. P. North, J. A. Lutz, D. J. Churchill, S. L. Roberts, D. F. Smith, R. J. McGaughey, J. T.
516 Kane, and M. L. Brooks. 2014. Assessing fire effects on forest spatial structure using a fusion of Landsat and
517 airborne LiDAR data in Yosemite National Park. *Remote Sensing of Environment* 151:89–101.
- 518 Kolb, T. E., C. J. Fettig, M. P. Ayres, B. J. Bentz, J. A. Hicke, R. Mathiasen, J. E. Stewart, and A. S. Weed.
519 2016. Observed and anticipated impacts of drought on forest insects and diseases in the United States. *Forest
520 Ecology and Management* 380:321–334.
- 521 Kuhn, M. 2008. Building Predictive Models in R Using the caret Package. *Journal of Statistical Software*
522 28:1–26.
- 523 Larson, A. J., and D. Churchill. 2012. Tree spatial patterns in fire-frequent forests of western North America,
524 including mechanisms of pattern formation and implications for designing fuel reduction and restoration
525 treatments. *Forest Ecology and Management* 267:74–92.
- 526 Li, W., Q. Guo, M. K. Jakubowski, and M. Kelly. 2012. A New Method for Segmenting Individual Trees
527 from the Lidar Point Cloud. *Photogrammetric Engineering & Remote Sensing* 78:75–84.
- 528 Logan, J. A., P. White, B. J. Bentz, and J. A. Powell. 1998. Model Analysis of Spatial Patterns in Mountain
529 Pine Beetle Outbreaks. *Theoretical Population Biology* 53:236–255.
- 530 Meyer, F., and S. Beucher. 1990. Morphological segmentation. *Journal of Visual Communication and Image*

- 531 Representation 1:21–46.
- 532 Micasense. 2015. MicaSense. <https://support.micasense.com/hc/en-us/articles/215261448-RedEdge-User-Manual-PDF-Download>
- 533 Miller, J. M., and F. P. Keen. 1960. Biology and control of the western pine beetle: A summary of the first
534 fifty years of research. US Department of Agriculture.
- 535 Moeck, H. A., D. L. Wood, and K. Q. Lindahl. 1981. Host selection behavior of bark beetles (Coleoptera:
536 Scolytidae) attacking *Pinus ponderosa*, with special emphasis on the western pine beetle, *Dendroctonus*
537 *brevicomis*. Journal of Chemical Ecology 7:49–83.
- 538 Morris, J. L., S. Cottrell, C. J. Fettig, W. D. Hansen, R. L. Sherriff, V. A. Carter, J. L. Clear, J. Clement, R.
539 J. DeRose, J. A. Hicke, P. E. Higuera, K. M. Mattor, A. W. R. Seddon, H. T. Seppä, J. D. Stednick, and S.
540 J. Seybold. 2017. Managing bark beetle impacts on ecosystems and society: Priority questions to motivate
541 future research. Journal of Applied Ecology 54:750–760.
- 542 Negrón, J. F., J. D. McMillin, J. A. Anhold, and D. Coulson. 2009. Bark beetle-caused mortality in a
543 drought-affected ponderosa pine landscape in Arizona, USA. Forest Ecology and Management 257:1353–1362.
- 544 North, M. P., S. L. Stephens, B. M. Collins, J. K. Agee, G. Aplet, J. F. Franklin, and P. Z. Fule. 2015.
545 Reform forest fire management. Science 349:1280–1281.
- 546 Pau, G., F. Fuchs, O. Sklyar, M. Boutros, and W. Huber. 2010. EBImagean R package for image processing
547 with applications to cellular phenotypes. Bioinformatics 26:979–981.
- 548 Pebesma, E., R. Bivand, E. Racine, M. Sumner, I. Cook, T. Keitt, R. Lovelace, H. Wickham, J. Ooms, K.
549 Müller, and T. L. Pedersen. 2019. Sf: Simple Features for R.
- 550 Plowright, A. 2018. ForestTools: Analyzing Remotely Sensed Forest Data.
- 551 Popescu, S. C., and R. H. Wynne. 2004. Seeing the Trees in the Forest: Using Lidar and Multispectral Data
552 Fusion with Local Filtering and Variable Window Size for Estimating Tree Height. PHOTOGRAMMETRIC
553 ENGINEERING:16.
- 554 Preisler, H. K., N. E. Grulke, Z. Heath, and S. L. Smith. 2017. Analysis and out-year forecast of beetle,
555 borer, and drought-induced tree mortality in California. Forest Ecology and Management. 399: 166-178
556 399:166–178.
- 557 R Core Team. 2018. R: A Language and Environment for Statistical Computing. R Foundation for Statistical
558 Computing, Vienna, Austria.
- 559 Raffa, K. F., and A. A. Berryman. 1983. The Role of Host Plant Resistance in the Colonization Behavior

- 560 and Ecology of Bark Beetles (Coleoptera: Scolytidae). Ecological Monographs 53:27–49.
- 561 Raffa, K. F., and A. A. Berryman. 1987. Interacting Selective Pressures in Conifer-Bark Beetle Systems: A
562 Basis for Reciprocal Adaptations? The American Naturalist 129:234–262.
- 563 Raffa, K. F., B. H. Aukema, B. J. Bentz, A. L. Carroll, J. A. Hicke, M. G. Turner, and W. H. Romme. 2008.
564 Cross-scale Drivers of Natural Disturbances Prone to Anthropogenic Amplification: The Dynamics of Bark
565 Beetle Eruptions. BioScience 58:501–517.
- 566 Raffa, K. F., J.-C. Grégoire, and B. Staffan Lindgren. 2015. Natural History and Ecology of Bark Beetles.
567 Pages 1–40 *in* Bark Beetles. Elsevier.
- 568 Rouse, W., R. H. Haas, W. Deering, and J. A. Schell. 1973. MONITORING THE VERNAL ADVANCEMENT
569 AND RETROGRADATION (GREEN WAVE EFFECT) OF NATURAL VEGETATION. Type II Report,
570 Goddard Space Flight Center, Greenbelt, MD, USA.
- 571 Roussel, J.-R. 2019. lidRplugins: Extra functions and algorithms for lidR package.
- 572 Roussel, J.-R., D. A. (. the documentation), F. D. B. (. bugs and improved catalog features), and A. S. M. (.
573 lassnags). 2019. lidR: Airborne LiDAR Data Manipulation and Visualization for Forestry Applications.
- 574 Seidl, R., J. Müller, T. Hothorn, C. Bässler, M. Heurich, and M. Kautz. 2016. Small beetle, large-scale
575 drivers: How regional and landscape factors affect outbreaks of the European spruce bark beetle. The Journal
576 of applied ecology 53:530–540.
- 577 Shiklomanov, A. N., B. A. Bradley, K. M. Dahlin, A. M. Fox, C. M. Gough, F. M. Hoffman, E. M. Middleton,
578 S. P. Serbin, L. Smallman, and W. K. Smith. 2019. Enhancing global change experiments through integration
579 of remote-sensing techniques. Frontiers in Ecology and the Environment 0.
- 580 Shin, P., T. Sankey, M. Moore, and A. Thode. 2018. Evaluating Unmanned Aerial Vehicle Images for
581 Estimating Forest Canopy Fuels in a Ponderosa Pine Stand. Remote Sensing 10:1266.
- 582 Stephenson, N. 1998. Actual evapotranspiration and deficit: Biologically meaningful correlates of vegetation
583 distribution across spatial scales. Journal of Biogeography 25:855–870.
- 584 Stephenson, N. L., A. J. Das, N. J. Ampersee, and B. M. Bulaon. 2019. Which trees die during drought?
585 The key role of insect host-tree selection. Journal of Ecology:75.
- 586 Thistle, H. W., H. Peterson, G. Allwine, B. Lamb, T. Strand, E. H. Holsten, and P. J. Shea. 2004. Surrogate
587 Pheromone Plumes in Three Forest Trunk Spaces: Composite Statistics and Case Studies. Forest Science 50.
- 588 USDAFS. 2019, February 11. Press Release: Survey finds 18 million trees died in California in 2018.

- 589 https://www.fs.usda.gov/Internet/FSE_DOCUMENTS/FSEPRD609321.pdf.
- 590 Vega, C., A. Hamrouni, S. El Mokhtari, J. Morel, J. Bock, J. P. Renaud, M. Bouvier, and S. Durrieu. 2014.
- 591 PTrees: A point-based approach to forest tree extraction from lidar data. International Journal of Applied
- 592 Earth Observation and Geoinformation 33:98–108.
- 593 Young, D. J. N., J. T. Stevens, J. M. Earles, J. Moore, A. Ellis, A. L. Jirka, and A. M. Latimer. 2017.
- 594 Long-term climate and competition explain forest mortality patterns under extreme drought. Ecology Letters
- 595 20:78–86.
- 596 Zhang, W., J. Qi, P. Wan, H. Wang, D. Xie, X. Wang, and G. Yan. 2016. An Easy-to-Use Airborne LiDAR
- 597 Data Filtering Method Based on Cloth Simulation. Remote Sensing 8:501.